High Power Laser Science and Engineering, (2024), Vol. 12, e23, 8 pages.
doi:10.1017/hpl.2024.2

HIGH POWER LASER SCIENCE AND ENGINEERING

RESEARCH ARTICLE

Compact mid-infrared dual-comb spectrometer over 3–4 μm via intra-pulse difference frequency generation in $LiNbO_3$ waveguides

Lian Zhou[1,†], Haipeng Lou[1,†], Zejiang Deng[1], Xiong Qin[1], Jiayi Pan[1], Yuanfeng Di[1], Chenglin Gu[1], Daping Luo[1], and Wenxue Li[1,2]

[1] *State Key Laboratory of Precision Spectroscopy, East China Normal University, Shanghai, China*

[2] *Joint Research Center of Light Manipulation Science and Photonic Integrated Chip of East China Normal University and Shandong Normal University, East China Normal University, Shanghai, China*

(Received 14 November 2023; revised 8 January 2024; accepted 15 January 2024)

Abstract

The mid-infrared optical frequency comb is a powerful tool for gas sensing. In this study, we demonstrate a simple mid-infrared dual-comb spectrometer covering 3–4 μm in $LiNbO_3$ waveguides. Based on a low-power fiber laser system, the mid-infrared comb is achieved via intra-pulse difference frequency generation in the $LiNbO_3$ waveguide. We construct pre-chirp management before supercontinuum generation to control spatiotemporal alignment for pump and signal pulses. The supercontinuum is directly coupled into a chirped periodically poled $LiNbO_3$ waveguide for the 3–4 μm idler generation. A mid-infrared dual-comb spectrometer based on this approach provides a 100 MHz resolution over 25 THz coverage. To evaluate the applicability for spectroscopy, we measure the methane spectrum using the dual-comb spectrometer. The measured results are consistent with the HITRAN database, in which the root mean square of the residual is 3.2%. This proposed method is expected to develop integrated and robust mid-infrared dual-comb spectrometers on chip for sensing.

Keywords: difference frequency generation; dual-comb spectroscopy; mid-infrared gas sensing; nonlinear optics

1. Introduction

Optical frequency combs are powerful tools for rapid gas sensing. In particular, frequency comb spectroscopy in the mid-infrared (MIR, 3–5 μm) region of the atmospheric window has made significant progress in various applications, such as greenhouse gas monitoring, atmospheric monitoring, green agriculture and breath analysis[1–4]. Generally, these MIR frequency combs can be obtained via $\chi^{(2)}$ and $\chi^{(3)}$ nonlinear processes in lithium niobate (LN)[5–9], which is a widely used optical material that can provide a wide transparency window, high nonlinear coefficient and electro-optical effect for integrated chip-based laser devices[10]. In comparison with bulk crystals, periodically poled LN (PPLN) waveguides with strong light confinement ensure high-efficiency nonlinear frequency conversion over a long interaction path. Therefore, PPLN waveguides allow low-power near-infrared (NIR) laser systems to perform efficient nonlinear processes and scale their spectra to the MIR region[11–14]. MIR sources based on LN waveguides have small size and low power consumption, making them ideal for the construction of integrated MIR frequency comb equipment. In addition, the dual-comb spectroscopy (DCS) system can realize high-resolution rapid spectral measurements by employing a single photodetector[15,16]. DCS combined with photonic technology can significantly reduce the equipment size and facilitate the development of portable gas sensors. Numerous integrated frequency combs based on microresonators, interband cascade lasers or diode lasers have been demonstrated for spectroscopy[17–19].

MIR spectroscopy offers high sensitivity for molecular sensing. However, limited spectral bandwidth and complex phase control pose two major challenges in demonstrating the technological advantages of DCS in the MIR region. To meet the bandwidth requirements, nonlinear conversion methods have been developed to broaden the spectra to the MIR region, including supercontinuum generation (SCG), difference frequency generation (DFG) and optical

Correspondence to: Daping Luo and Wenxue Li, State Key Laboratory of Precision Spectroscopy, East China Normal University, Shanghai 200062, China. Email: dpluo@lps.ecnu.edu.cn (D. Luo); wxli@phy.ecnu.edu.cn (W. Li)

[†]These authors contributed equally to this work.

parametric oscillators (OPOs)[20]. State-of-the-art broadband MIR dual-comb systems have been achieved via DFG and OPOs, which have also been successfully applied in comb-line-resolved DCS and multispecies detection of trace gases[21–24]. Generally, the DFG system, which can passively stabilize the carrier-envelope phase of the MIR comb, consists of the noncollinear pump and signal branches from the same seed laser. In this two-branch structure, delay control is required to stabilize the pump-signal pulse walk-off in the time domain and suppress the intensity noise of MIR pulses[25]. Recently, several studies have reported the simple method of MIR comb generation via intra-pulse DFG (IPDFG)[26–30]. Through precise chirp management of the supercontinuum, a single branch can provide natural spatiotemporal alignment for the pump and signal pulses, achieving multi-octave-spanning MIR combs[26–28]. The potential of these simple IPDFG MIR systems for high-resolution DCS has been demonstrated in the past[29,30]. By combining the IPDFG and PPLN waveguides, a broadband MIR comb source was realized with an integrated and simple structure[31]. Therefore, we believe that a portable gas-sensing instrument can be developed using DCS and IPDFG combs on an LN waveguide.

In this study, a simple 3–4 μm MIR dual-comb spectrometer with waveguide-based IPDFG modules is demonstrated. We constructed an Er-doped fiber dual-comb system as the seed source. To realize the spatiotemporal alignment of the pump and signal pulses, the front prism pair provides easily adjustable pre-chirp control for the soliton self-compression in a highly nonlinear fiber (HNLF). The broadband MIR combs over the 3–4 μm region were yielded from high-efficiency chirped PPLN waveguides via the IPDFG process. Thereafter, comb-line-resolved DCS with 100 MHz spectral resolution over 25 THz coverage was demonstrated. Finally, we measured the absorption spectrum of methane to verify the applicability of the MIR dual-comb system for precision spectroscopy. We compared the measured result with the HITRAN database, and the root mean square (RMS) of the residual is 3.2%. This dual-comb system without phase correction enables mode-resolved DCS with a figure of merit of 1.03×10^6. Thus far, femtosecond lasers, frequency combs, amplifiers and SCG on chips have been successfully demonstrated[32–34]. The MIR comb generation method, which does not require the detection of the offset frequency of MIR pulses, is conducive to low-power sources on chips. We believe that this approach contributes to the development of broadband MIR frequency combs and portable DCS systems on chips.

2. Experimental setup and results

The schematic of the MIR comb generation is shown in Figure 1, which includes a seed comb centered at 1.5 μm, an Er-doped fiber amplifier, a prism compressor, an HNLF, and an IPDFG module. The seed comb based on an Er-doped fiber mode-locked laser emitted a pulse train with 1 mW average power and a 100 MHz repetition rate. The average pulse power was scaled up to 328 mW using a bidirectionally pumped fiber amplifier, in which a 3 m Er-doped single-mode fiber with a normal dispersion was used as the gain medium. A pair of silicon prisms was adopted to provide controllable anomalous dispersion for pre-chirp management of SCG. Linearly polarized light was injected into the dispersion prisms at a Brewster angle to reduce the reflection loss on the prism surfaces. Behind the prism compression, a 300 mW laser was coupled to a collimator with a 12 cm PM1550 pigtail fiber, which could further recompress the pulse duration. Figures 2(a) and 2(b) show the autocorrelation curve and spectrum after the prism compressor, respectively. The pulse duration is 92 fs with sech^2 fitting, and the spectrum covers the range from 1520 to 1620 nm. The large pulse wings are caused by uncompensated nonlinear chirp. A 3 cm PM HNLF with an anomalous dispersion of 1.9 ps/(nm·km) was employed to generate a

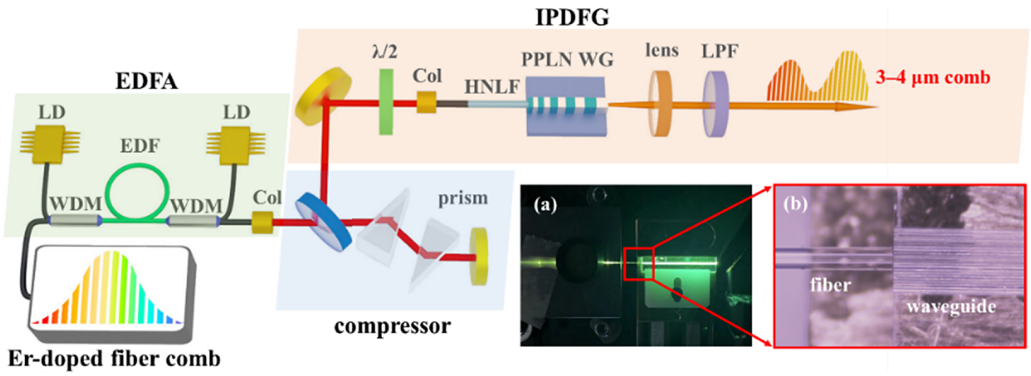

Figure 1. Schematic of the MIR comb generation. The lens after the waveguide is to make the schematic easier to understand. In the actual system, we use an off-axis parabolic mirror to collimate the MIR light instead of the lens. LD, laser diode; EDF, Er-doped fiber; WDM, wavelength division multiplexer; Col, collimator; EDFA, Er-doped fiber amplifier; λ/2, half-wave plate; HNLF, highly nonlinear fiber; PPLN WG, periodically poled lithium niobate waveguide; and LPF, long-pass filter. Moreover, we also recorded the images of the PPLN WG using a phone camera (inset (a)) and a charge-coupled device (CCD) camera (inset (b)).

https://doi.org/10.1017/hpl.2024.2 Published online by Cambridge University Press

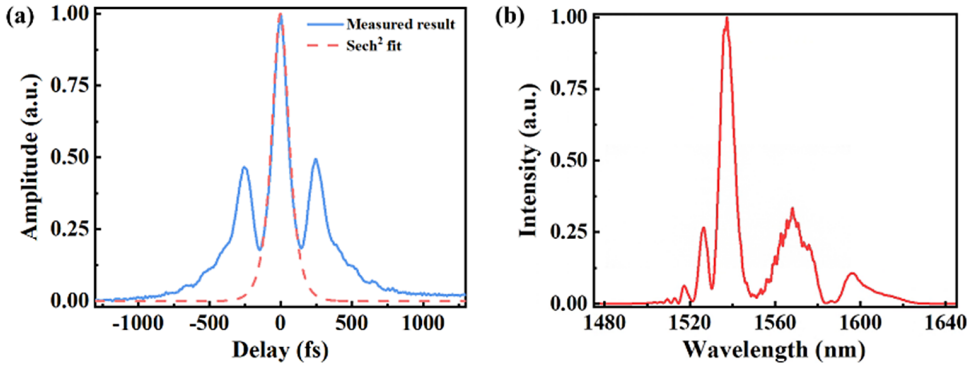

Figure 2. (a) Autocorrelation trace and (b) measured spectrum of the compressor output.

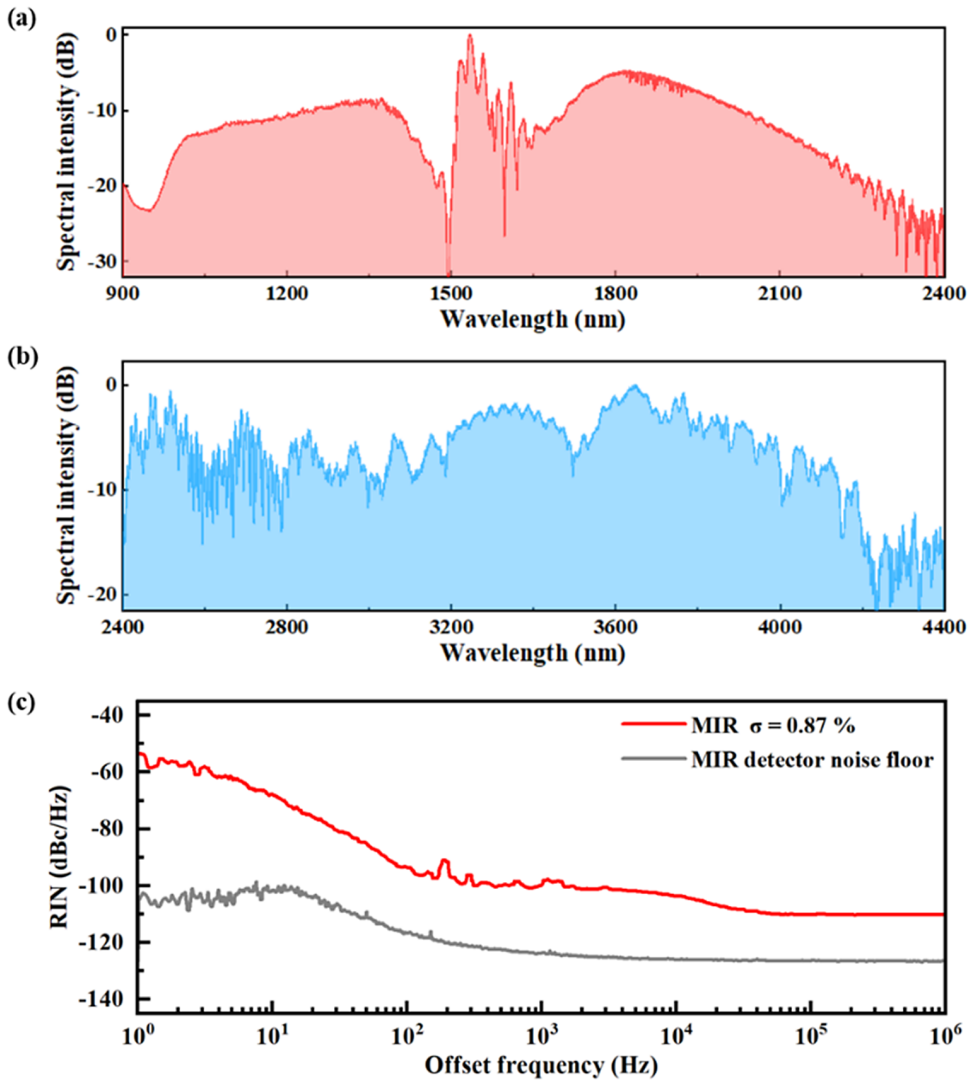

Figure 3. (a) Spectral profile of SCG. The spectral region is separately measured using a Yokogawa AQ6370 (900–1700 nm) and a Bristol 771B (1700–2400 nm). (b) Spectral profile of the MIR comb. (c) RIN of MIR light.

supercontinuum spectrum. The spectral broadening and soliton self-compression processes in the anomalous-dispersion HNLF were adjusted using the prism-based pre-chirp management module.

To drive the IPDFG and yield MIR light, the supercontinuum from the HNLF was directly coupled to a chirped PPLN waveguide. The HNLF is placed on a three-axis stage to launch light to the waveguide. A zoom lens and a camera

https://doi.org/10.1017/hpl.2024.2 Published online by Cambridge University Press

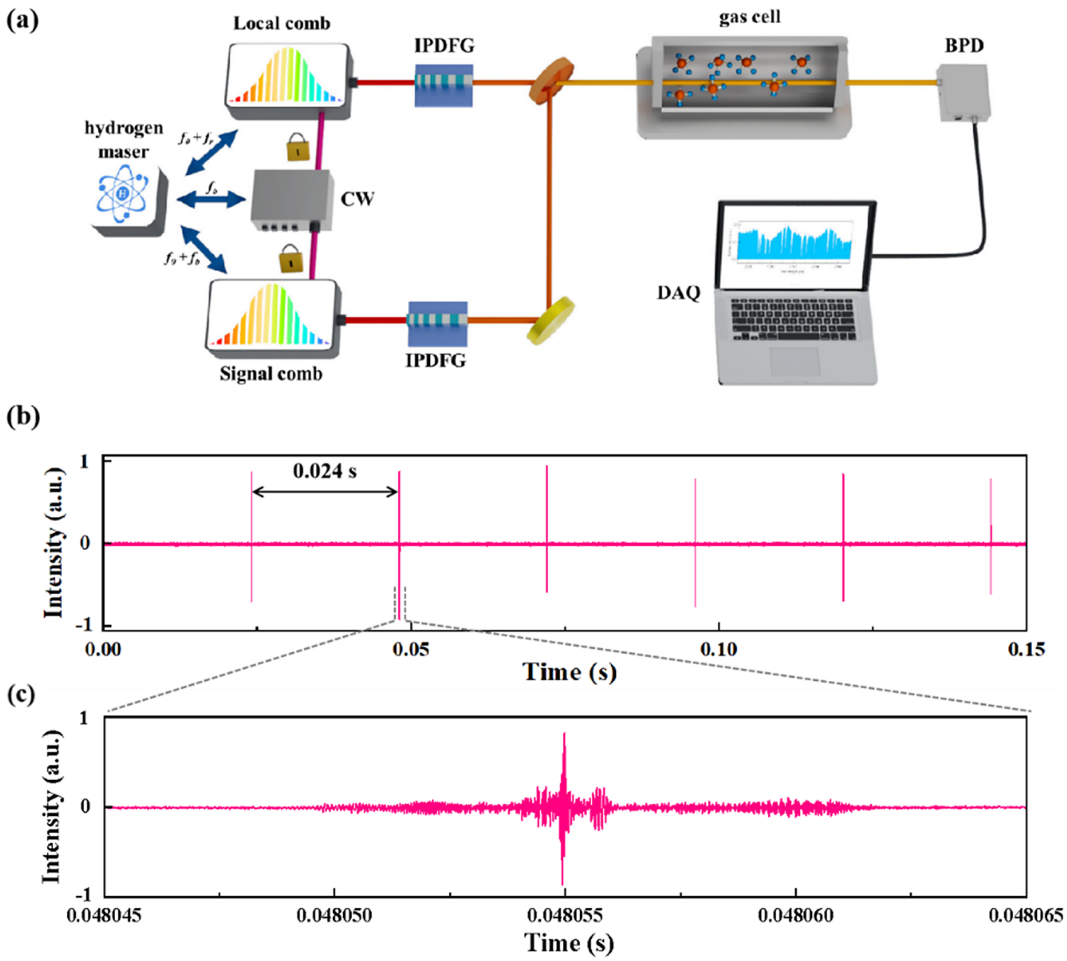

Figure 4. (a) Schematic of the MIR dual-comb system. The recorded interferograms at different time scales of (b) 150 ms and (c) 0.02 ms. CW, continuous-wave laser; BPD, balanced photodetector; DAQ, data acquisition.

system on the top of the waveguide were used for high-magnification imaging. By adjusting the stage, we can get the optimal alignment and measure the output light. The mode diameter of the HNLF is 3.5 μm. This PPLN waveguide is 15 μm wide and 25 mm long with aperiodic periods of 23–32 μm that were consistent with our previous study[35]. The coupling efficiency is 60%. In general, some spatial optical components, including wedge and chirp mirrors, were required to control the pulse chirp before IPDFG[26,28]. These extra spatially manipulated modules increased total loss and system complexity. In particular, we did not adopt common methods for controlling the chirp but simply adjusted the prism pair before the anomalous-dispersion HNLF to optimize the temporal alignment of pump-signal pulses with the soliton self-compression effect[27,36–38]. In addition, these prisms could be removed completely to simplify the system for integrated MIR comb generation[31]. Thereafter, a gold-coated off-axis parabolic mirror with a focal distance of 6 mm collimated the light to free space. Finally, a long-pass filter at 2.4 μm was used to filter out the residual pump and signal light, outputting an MIR frequency comb with high transmissivity.

To characterize the spectral evolution of the SCG and IPDFG, we measured the corresponding spectral profiles using two commercial spectrometers (Yokogawa AQ6370 and Bristol 771B). The HNLF delivers a 150 mW supercontinuum with a spectral range of 1–2 μm, as shown in Figure 3(a). Theoretically, this supercontinuum spectrum can provide the pump and signal light for 2–5 μm idler generation. In addition, absorption lines were observed at approximately 1900 nm owing to water vapor in the air. To maximize the conversion efficiency of the IPDFG, the slow axis of the HNLF was rotated to ensure that the pump and signal lights were coupled to the waveguide with vertical polarization. After the filter, 0.7 mW MIR light was obtained. The spectrum was measured using a Fourier-transform spectrometer (Bristol 771B) with a 33 GHz spectral resolution, as shown in Figure 3(b). We observed that the long wavelength was cut off at 4.2 μm, which was not as broad as expected. The most likely reason is that the waveguide channel brought different group velocity dispersions to the pump and signal pulses, which caused temporal misalignment of the pump and signal pulses. In addition, the effect of waveguide dispersion on the refractive index

https://doi.org/10.1017/hpl.2024.2 Published online by Cambridge University Press

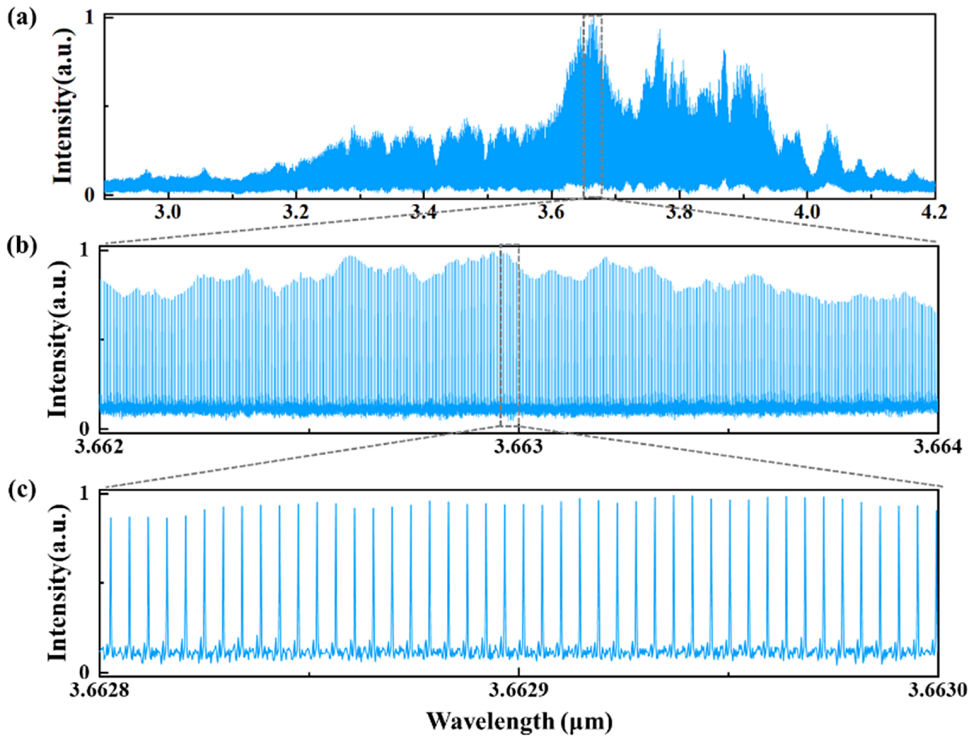

Figure 5. Mode-resolved MIR dual-comb spectra at different wavelength scales of (a) 1.4 μm, (b) 0.002 μm and (c) 0.0002 μm.

is ignored, so the poling periods are not optimal. In future studies, dispersion engineering and poling periods should be considered to redesign the waveguide and broaden the MIR spectrum[39]. We measured the relative intensity noise (RIN) of the MIR light, as shown in Figure 3(c). The integrated RIN is 0.87%.

A dual-comb spectrometer based on the IPDFG method was constructed for DCS measurement, as shown in Figure 4(a). Two Er-doped fiber comb systems served as the seed combs. The NIR local comb (f_{0_comb1} = 20 MHz and f_{r_comb1} = 100 MHz) was referenced to the hydrogen maser clock. A 10 Hz linewidth continuous-wave (CW) laser centered at 1560 nm (OE4030, OEwaves) was referenced to the local comb to provide a standard optical frequency reference for the signal comb. To stabilize the signal comb, the carrier-envelope-phase offset frequency (f_{0_comb2} = 20 MHz) and the optical beat note were locked. Moreover, two electro-optic modulators were used in the signal oscillator to improve the modulation bandwidth of the frequency control[40]. Thereafter, two combs were delivered into two parallel IPDFG modules to generate the MIR dual-comb system. The two MIR combs could provide a broad spectrum from 2.4 to 4.2 μm. To evaluate the applicability for spectroscopy, the two MIR beams were combined to pass through an 8 cm gas cell filled with pure methane at a pressure of 150 mbar. The interferogram signal was acquired through a balanced photodetector (Qube-DT, ppqSense) equipped with two HgCdTe photodetectors (PVI-2TE-5, VIGO System). The response spectral range of the detector is 3–5 μm. In addition, two half-wavelength plates were used to control the polarization of the MIR light and optimize the signal-to-noise ratio (SNR) of the interferograms. Before the detection, we attenuated the power of the signal comb to ensure that the two beams with the same power were injected into the detector. After passing through a 48 MHz electronic low-pass filter, the DCS signal was recorded using a data acquisition card with a sampling rate of 100 MHz. Figure 4(b) shows the measured interferogram signal for 150 ms. It is evident that the period of the interferograms was approximately 0.024 s, corresponding to the repetition rate difference of approximately 42 Hz. Figure 4(c) exhibits a 0.02 ms temporal domain of interferograms in which we can acquire the information in the frequency domain via further Fourier transform.

To retrieve the frequency-domain optical spectrum, 20 interferograms (0.5-s temporal signal) were extracted as a unit for the Fourier transform. To obtain a high SNR DCS, the frequency domain was coherently averaged by 208 times over 100 s. As illustrated in Figure 5(a), we obtained the DCS in the range of 3.0–4.2 μm, corresponding to a frequency bandwidth of 25 THz. The retrieved dual-comb spectrum was narrower than the spectrum measured using a Fourier-transform spectrometer because we could not retrieve the spectrum in the 2–3 μm range owing to the limited response bandwidth (3–5 μm) of the detector. In the frequency domain, approximately 2.5 × 10^5 modes were resolved with a 100 MHz spectral resolution. We also calculated the figure of merit, defined as SNR × M / $T^{1/2}$,

https://doi.org/10.1017/hpl.2024.2 Published online by Cambridge University Press

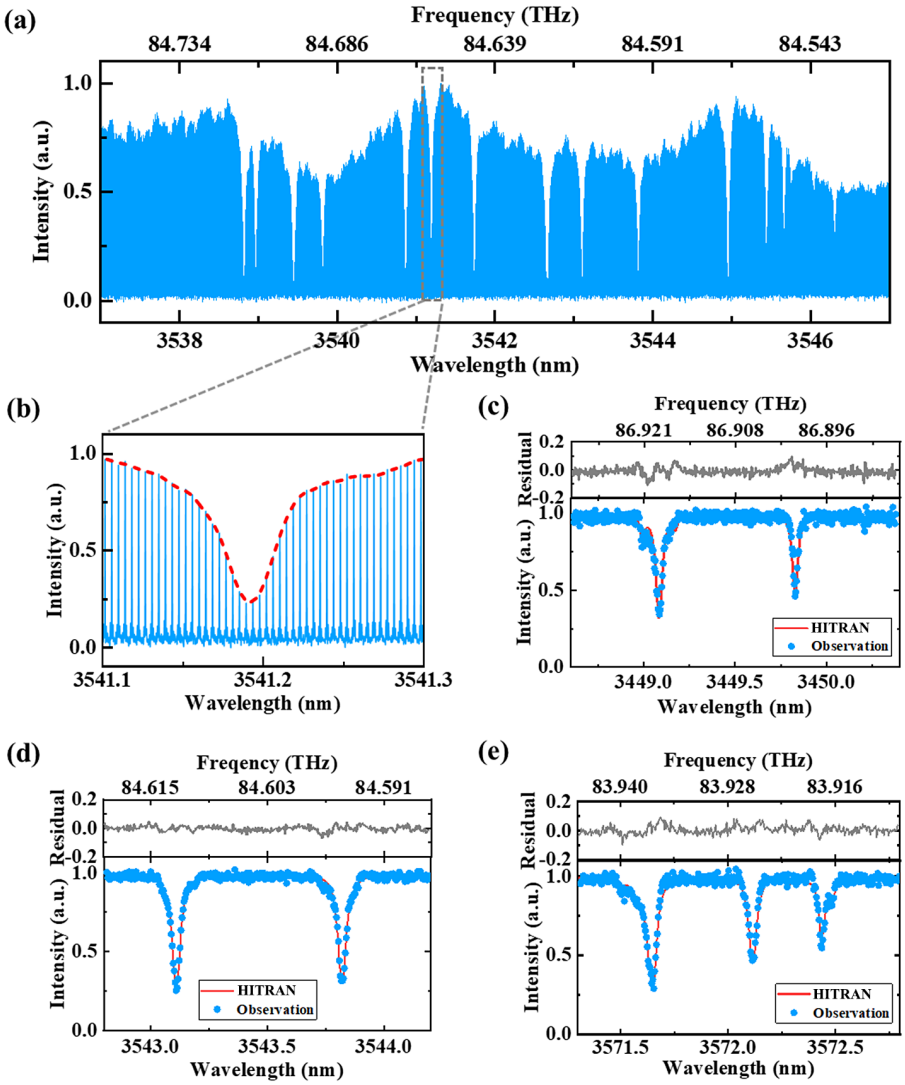

Figure 6. (a) Absorption lines of methane in the 3537–3547 nm region. (b) Zoom-in absorption line of methane at 3541.1–3541.3 nm. (c)–(e) Comparison results of the extracted gas absorption lines (blue dot) and the theoretical profiles from the HITRAN database (red line).

where M is the number of comb teeth and T is the measurement time. The figure of merit was 1.03×10^6, which is with the same order of magnitude as the results in Refs. [30,41]. In addition, the SNR of the peak spectrum, which represents the ratio of the signal to random variations of the baseline[21], was 28. Figures 5(b) and 5(c) show the mode-resolved MIR dual-comb spectra over wavelength spans of 0.002 and 0.0002 μm, respectively, confirming that the simple DCS system has the capacity for high-resolution gas sensing in the MIR region.

To assess the applicability of the MIR dual-comb system to high-resolution spectroscopy, we measured its methane absorption spectrum. Several absorption lines in the 3537–3547 nm region are shown in Figure 6(a). A single absorption peak zoom-in in the 3541.1–3541.3 nm range consists of approximately 50 comb modes with a frequency interval of approximately 100 MHz, as shown in Figure 6(b). Figures 6(c)–6(e) show several absorption peaks (blue dots), in which all the absorption lines are consistent with the standard profiles (red curves, Voigt profiles, HITRAN 2020[42]). The RMSs of the residuals in Figures 6(c)–6(e) were 3.2%, 1.9% and 2.9%, respectively.

In the low SNR range, it is difficult to retrieve the absorption lines, although the SNR of our system can be further improved by increasing the power. The saturation power (~2 mW) of the detector limited the SNR because each comb line has only nW-level power. It remains a challenge for dual-comb systems to achieve high SNR DCS in broadband parallel measurement. Recent work has demonstrated a method of signal processing to resolve this issue in the NIR region, and the ideas could be used to improve the SNR of MIR DCS[43]. In this system, the spectrum has a fast baseline with tens of gigahertz linewidth, which is a similar linewidth to that with the gas absorption line at standard or high atmospheric pressure. So, we measure the gas absorption peak at low pressure (150 mbar) to reduce

https://doi.org/10.1017/hpl.2024.2 Published online by Cambridge University Press

the impact of the baseline. For broader absorption lines at standard atmospheric pressure, the four-point normalization correction method can be used to effectively remove the effects of the baseline[1,41,44].

3. Conclusion

We demonstrated a simple and compact MIR dual-comb spectrometer. Using the IPDFG method, we yielded broad MIR combs on chirped PPLN waveguides and developed a mode-resolved dual-comb spectrometer. The spectrometer provided 100 MHz resolution in the range of 3.0–4.2 μm corresponding to 25 THz bandwidth. In comparison with bulky two-branch DFG combs, the proposed MIR comb system is not only more integrated but also more stable, without noise from the pump-signal delay jitter. The high-efficiency PPLN waveguide reduced the power threshold required to drive the IPDFG process. In addition, the lens group for waveguide coupling could be replaced by an all-fiber structure. Optimization of the period distribution and channel length of the waveguide would improve the MIR spectral bandwidth. This MIR dual-comb system is expected to develop into more integrated measurement devices with on-chip femtosecond pulse generation, amplifiers and nonlinear broadening technologies for portable gas-sensing equipment with high sensitivity and high resolution.

Acknowledgement

This work was supported in part by the National Natural Science Foundation of China (Nos. 12204178, 12104162, 12134004 and 12274141).

References

1. G. Ycas, F. R. Giorgetta, K. C. Cossel, E. M. Waxman, E. Baumann, N. R. Newbury, and I. Coddington, Optica **6**, 165 (2019).
2. F. R. Giorgetta, J. Peischl, D. I. Herman, G. Ycas, I. Coddington, N. R. Newbury, and K. C. Cossel, Laser Photonics Rev. **15**, 2000583 (2021).
3. D. I. Herman, C. Weerasekara, L. C. Hutcherson, F. R. Giorgetta, K. C. Cossel, E. M. Waxman, G. M. Colacion, N. R. Newbury, S. M. Welch, B. D. DePaola, I. Coddington, E. A. Santos, and B. R. Washburn, Sci. Adv. **7**, eabe9765 (2021).
4. Q. Liang, Y.-C. Chan, J. Toscano, K. K. Bjorkman, L. A. Leinwand, R. Parker, E. S. Nozik, D. J. Nesbitt, and J. Ye, J. Breath Res. **17**, 036001 (2023).
5. D. L. Maser, G. Ycas, W. I. Depetri, F. C. Cruz, and S. A. Diddams, Appl. Phys. B **123**, 142 (2017).
6. F. C. Cruz, D. L. Maser, T. Johnson, G. Ycas, A. Klose, F. R. Giorgetta, I. Coddington, and S. A. Diddams, Opt. Express **23**, 26814 (2015).
7. L. Nitzsche, J. Goldschmidt, J. Kiessling, S. Wolf, F. Kühnemann, and J. Wöllenstein, Opt. Express **29**, 25449 (2021).
8. G. Soboń, T. Martynkien, P. Mergo, L. Rutkowski, and A. Foltynowicz, Opt. Lett. **42**, 1748 (2017).
9. C. P. Bauer, S. L. Camenzind, J. Pupeikis, B. Willenberg, C. R. Phillips, and U. Keller, Opt. Express **30**, 19904 (2022).
10. A. Boes, L. Chang, C. Langrock, M. Yu, M. Zhang, Q. Lin, M. Lončar, M. Fejer, J. Bowers, and A. Mitchell, Science **379**, eabj4396 (2023).
11. J. Lu, J. B. Surya, X. Liu, Y. Xu, and H. X. Tang, Opt. Lett. **44**, 1492 (2019).
12. H. Guo, B. Zhou, X. Zeng, and M. Bache, Opt. Express **22**, 12211 (2014).
13. S. Kowligy, A. Lind, D. D. Hickstein, D. R. Carlson, H. Timmers, N. Nader, F. C. Cruz, G. Ycas, S. B. Papp, and S. A. Diddams, Opt. Lett. **43**, 1678 (2018).
14. M. Liu, R. M. Gray, L. Costa, C. R. Markus, A. Roy, and A. Marandi, Nat. Commun. **14**, 1044 (2023).
15. N. Picqué, and T. W. Hänsch, Nat. Photonics **13**, 146 (2019).
16. I. Coddington, N. Newbury, and W. Swann, Optica **3**, 414 (2016).
17. C. Bao, Z. Yuan, L. Wu, M.-G. Suh, H. Wang, Q. Lin, and K. J. Vahala, Nat. Commun. **12**, 6573 (2021).
18. L. A. Sterczewski, T.-L. Chen, D. C. Ober, C. R. Markus, C. L. Canedy, I. Vurgaftman, C. Frez, J. R. Meyer, M. Okumura, and M. Bagheri, ACS Photonics **9**, 994 (2022).
19. L. A. Sterczewski, M. Fradet, C. Frez, S. Forouhar, and M. Bagheri, Laser Photonics Rev. **17**, 2200224 (2022).
20. M. L. Weichman, P. B. Changala, J. Ye, Z. Chen, M. Yan, and N. Picqué, J. Mol. Spectrosc. **355**, 66 (2019).
21. G. Ycas, F. R. Giorgetta, E. Baumann, I. Coddington, D. Herman, S. A. Diddams, and N. R. Newbury, Nat. Photonics **12**, 202 (2018).
22. V. Muraviev, V. O. Smolski, Z. E. Loparo, and K. L. Vodopyanov, Nat. Photonics **12**, 209 (2018).
23. S. Vasilyev, A. Muraviev, D. Konnov, M. Mirov, V. Smolski, I. Moskalev, S. Mirov, and K. Vodopyanov, Opt. Lett. **48**, 2273 (2023).
24. T. Tomberg, A. Muraviev, Q. Ru, and K. L. Vodopyanov, Optica **6**, 147 (2019)
25. S. Oliveira, A. Ruehl, P. Masłowski, and I. Hartl, Opt. Lett. **45**, 1914 (2020).
26. D. M. B. Lesko, H. Timmers, S. Xing, A. Kowligy, A. J. Lind, and S. A. Diddams, Nat. Photonics **15**, 281 (2021).
27. S. Xing, D. M. B. Lesko, T. Umeki, A. J. Lind, N. Hoghooghi, T.-H. Wu, and S. A. Diddams, APL Photonics **6**, 086110 (2021).
28. N. Hoghooghi, S. Xing, P. Chang, D. Lesko, A. Lind, G. Rieker, and S. Diddams, Light Sci. Appl. **11**, 264 (2022).
29. J. Lind, A. Kowligy, H. Timmers, F. C. Cruz, N. Nader, M. C. Silfies, T. K. Allison, and S. A. Diddams, Phys. Rev. Lett. **124**, 133904 (2020).
30. H. Timmers, A. Kowligy, A. Lind, F. C. Cruz, N. Nader, M. Silfies, G. Ycas, T. K. Allison, P. G. Schunemann, S. B. Papp, and S. A. Diddams, Optica **5**, 727 (2018).
31. K. Iwakuni, S. Okubo, O. Tadanaga, H. Inaba, A. Onae, F.-L. Hong, and H. Sasada, Opt. Lett. **41**, 3980 (2016).
32. M. Yu, D. Barton III, R. Cheng, C. Reimer, P. Kharel, L. He, L. Shao, D. Zhu, Y. Hu, H. R. Grant, L. Johansson, Y. Okawachi, A. L. Gaeta, M. Zhang, and M. Lončar, Nature **612**, 252 (2022).
33. J. Zhou, Y. Liang, Z. Liu, W. Chu, H. Zhang, D. Yin, Z. Fang, R. Wu, J. Zhang, W. Chen, Z. Wang, Y. Zhou, M. Wang, and Y. Cheng, Laser Photon. Rev. **15**, 2100030 (2021).
34. B. Kuyken, T. Ideguchi, S. Holzner, M. Yan, T. W. Hänsch, J. V. Campenhout, P. Verheyen, S. Coen, F. Leo, R. Baets, G. Roelkens, and N. Picqué, Nat. Commun. **6**, 6310 (2015).
35. L. Zhou, Y. Liu, H. Lou, Y. Di, G. Xie, Z. Zhu, Z. Deng, D. Luo, C. Gu, H. Chen, and W. Li, Opt. Lett. **45**, 6458 (2020).
36. J. C. Travers, T. F. Grigorova, C. Brahms, and F. Belli, Nat. Photonics **13**, 547 (2019).
37. S. Xing, A. S. Kowligy, D. M. B. Lesko, A. J. Lind, and S. A. Diddams, Opt. Lett. **45**, 2660 (2020).

https://doi.org/10.1017/hpl.2024.2 Published online by Cambridge University Press

38. Z. Li, C. Yao, Z. Jia, F. Wang, G. Qin, Y. Ohishi, and W. Qin, Appl. Phys. Lett. **115**, 091103 (2019).
39. M. Jankowski, C. Langrock, B. Desiatov, A. Marandi, C. Wang, M. Zhang, C. R. Phillips, M. Lončar, and M. M. Fejer, Optica **7**, 40 (2020).
40. Z. Deng, Y. Liu, Z. Zhu, D. Luo, C. Gu, L. Zhou, G. Xie, and W. Li, Opt. Laser Technol. **138**, 106906 (2021).
41. G. Ycas, F. R. Giorgetta, J. T. Friedlein, D. Herman, K. C. Cossel, E. Baumann, N. R. Newbury, and I. Coddington, Opt. Express **28**, 14740 (2020).
42. E. Gordon, L. S. Rothman, R. J. Hargreaves, R. Hashemi, E. V. Karlovets, F. M. Skinner, E. K. Conway, C. Hill, R. V. Kochanov, Y. Tan, P. Wcisło, A. A. Finenko, K. Nelson, P. F. Bernath, M. Birk, V. Boudon, A. Campargue, K. V. Chance, A. Coustenis, B. J. Drouin, J.-M. Flaud, R. R. Gamache, J. T. Hodges, D. Jacquemart, E. J. Mlawer, A. V. Nikitin, V. I. Perevalov, M. Rotger, J. Tennyson, G. C. Toon, H. Tran, V. G. Tyuterev, E. M. Adkins, A. Baker, A. Barbe, E. Canè, A. G. Császár, A. Dudaryonok, O. Egorov, A. J. Fleisher, H. Fleurbaey, A. Foltynowicz, T. Furtenbacher, J. J. Harrison, J.-M. Hartmann, V.-M. Horneman, X. Huang, T. Karman, J. Karns, S. Kassi, I. Kleiner, V. Kofman, F. Kwabia-Tchana, N. N. Lavrentieva, T. J. Lee, D. A. Long, A. A. Lukashevskaya, O. M. Lyulin, V. Y. Makhnev, W. Matt, S. T. Massie, M. Melosso, S. N. Mikhailenko, D. Mondelain, H. S. P. Müller, O. V. Naumenko, A. Perrin, O. L. Polyansky, E. Raddaoui, P. L. Raston, Z. D. Reed, M. Rey, C. Richard, R. Tóbiás, I. Sadiek, D. W. Schwenke, E. Starikova, K. Sung, F. Tamassia, S. A. Tashkun, J. Vander Auwera, I. A. Vasilenko, A. A. Vigasin, G. L. Villanueva, B. Vispoel, G. Wagner, A. Yachmenev, and S. N. Yurchenko, J. Quant. Spectrosc. Radiat. Transfer **277**, 107949 (2022).
43. P. Guay, M. Walsh, A. Tourigny-Plante, and J. Genest, Opt. Express **31**, 4393 (2023).
44. G. B. Rieker, F. R. Giorgetta, W. C. Swann, J. Kofler, A. M. Zolot, L. C. Sinclair, E. Baumann, C. Cromer, G. Petron, C. Sweeney, P. P. Tans, I. Coddington, and N. R. Newbury, Optica **1**, 290 (2014).

https://doi.org/10.1017/hpl.2024.2 Published online by Cambridge University Press